Lanthanide ion-doped silica nanohelix: a helical inorganic network acts as a chiral source for metal ions

Tomoyuki Harada, Hiroshi Yanagita, Naoya Ryu, Yutaka Okazaki, Yutaka Kuwahara, Makoto Takafuji, Shoji Nagaoka, Hirotaka Ihara, Reiko Oda

▶ **To cite this version:**

Tomoyuki Harada, Hiroshi Yanagita, Naoya Ryu, Yutaka Okazaki, Yutaka Kuwahara, et al.. Lanthanide ion-doped silica nanohelix: a helical inorganic network acts as a chiral source for metal ions. Chemical Communications, 2021, 57 (36), pp.4392 - 4395. ⟨10.1039/d1cc01112j⟩. ⟨hal-03860012⟩

HAL Id: hal-03860012

https://hal.science/hal-03860012v1

Submitted on 18 Nov 2022

HAL is a multi-disciplinary open access archive for the deposit and dissemination of scientific research documents, whether they are published or not. The documents may come from teaching and research institutions in France or abroad, or from public or private research centers.

L'archive ouverte pluridisciplinaire **HAL**, est destinée au dépôt et à la diffusion de documents scientifiques de niveau recherche, publiés ou non, émanant des établissements d'enseignement et de recherche français ou étrangers, des laboratoires publics ou privés.

HAL Authorization

Lanthanide ion-doped silica nanohelix: a helical inorganic network acts as a chiral source for metal ions†

Tomoyuki Harada,[a] Hiroshi Yanagita,[a] Naoya Ryu,[*b] Yutaka Okazaki,[c] Yutaka Kuwahara,[a] Makoto Takafuji,[a] Shoji Nagaoka,[ab] Hirotaka Ihara[*a] and Reiko Oda[*d]

We demonstrate that lanthanide ions doped in nanometrical silica helices with a chirally arranged siloxane network without any organic mediates show induced chiroptical properties such as circular dichroism and circularly polarized luminescence.

In nature, many living objects are based on chiral components. We researchers utilize them, mimic them, are inspired by them, and have developed functional materials with chiral properties. Not only do they have interesting properties based on their intrinsic chiral properties, but chiral matter can also induce such properties to non-chiral matter, allowing us to design novel functional chiral materials. There are many examples on chirality induction in originally non-chiral organic molecules/polymers[1] and inorganic solids[2,3] by chiral organic molecules/polymers. Recent reports including ours show that chiral inorganic solids can also induce chiral properties in originally non-chiral organic molecules[3,4] and inorganic solids (nanoparticles or nanoclusters).[5–7] In most of these examples, organic mediates are used as a linker or an adsorbent for chirality induction in inorganic nanosolids by inorganic solids. Compared to these inorganic nanosolids, metal ions have different properties. In particular, metal ions with chiral properties are very attractive due to their promising applications in asymmetric catalysis,[8] chiral recognition[9] and chiroptical properties.[10] However, until now, the chiral sources for metal ions have been limited to organic molecules/polymers.[8–10] For almost two decades, our group has established a sol–gel preparation method of twisted and helical silica nanoribbons templated from surfactant self-assemblies.[4,6,7,11–13] Several years ago, we showed that such silica nanohelices have a chirally arranged siloxane network without any organic templates as evidenced by the vibrational circular dichroism analysis.[7,13] In the present work, we asked ourselves whether such inorganic solids with a chiral network could act as chiral ligands for metal ions entrapped within in the absence of organic mediates.

It is well known that some lanthanide ions serve as a fluorescent source in metal oxide matrices.[14–17] Therefore, we chose here to dope lanthanide ions into the helical and twisted silica nanoribbons and investigated the effect of the presence of a chiral siloxane network on the optical properties of such ions. Fig. 1 shows a schematic representation of the preparation procedure of the lanthanide ion-doped silica nanohelices. Right- or left-handed nanohelices were prepared from cationic gemini surfactant, *N*,*N*′-dihexadecyl-*N*,*N*,*N*′,*N*′-tetramethylethylene diammonium L- or D-tartrate (hereafter, abbreviated as 16-2-16 L- and D-tartrate), respectively, as shown in our previous reports.[4,6,7,11–13] The presence of self-assembled 16-2-16 L- and D-tartrate nanohelices as well as silica nanohelices after polycondensation of tetraethyl orthosilicate was confirmed by scanning

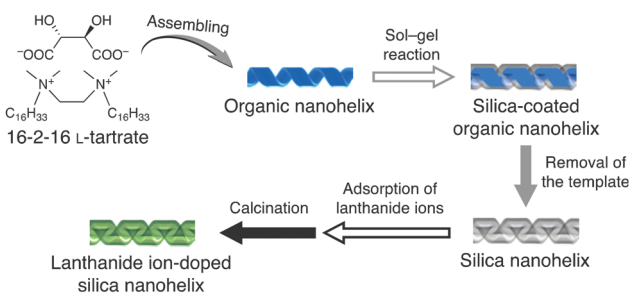

Fig. 1 Schematic illustration of the preparation procedure of lanthanide ion-doped silica nanohelices.

[a] *Department of Applied Chemistry and Biochemistry, Kumamoto University, 2-39-1 Kurokami, Chuo-ku Kumamoto 860-8555, Japan. E-mail: ihara@kumamoto-u.ac.jp*
[b] *Materials Development Department, Kumamoto Industrial Research Institute, 3-11-38 Higashimachi, Higashi-ku, Kumamoto 862-0901, Japan. E-mail: n-ryu@kumamoto-iri.jp*
[c] *International Research and Education Centre of Advanced Energy Science, Graduate School of Energy Science, Kyoto University, Yoshida-Honmachi, Sakyo-ku Kyoto 606-8501, Japan*
[d] *Institut de Chimie & Biologie des Membranes & des Nano-objets (UMR5248 CBMN), CNRS, Université de Bordeaux, Institut Polytechnique Bordeaux 2 rue Robert Escarpit, Pessac 33607, France. E-mail: reiko.oda@u-bordeaux.fr*

† Electronic supplementary information (ESI) available: Experimental details, supplementary figures and author contributions. See DOI: 10.1039/d1cc01112j

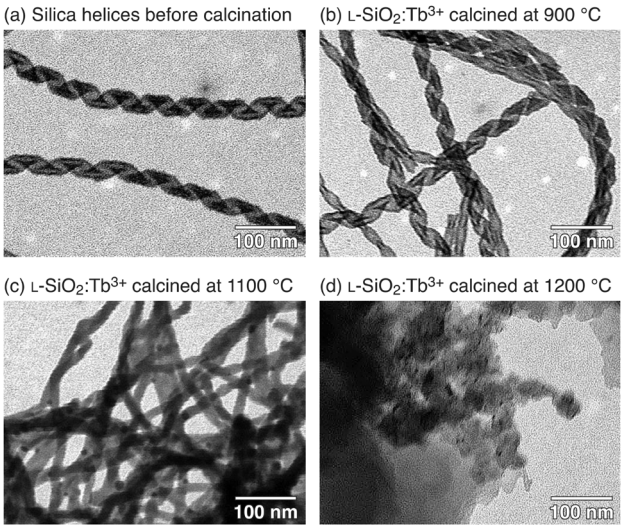

Fig. 2 STEM images of (a) silica nanohelices prepared from 16-2-16 L-tartrate without calcination and L-SiO_2:Tb^{3+}s calcined at (b) 900, (c) 1100 and (d) 1200 °C.

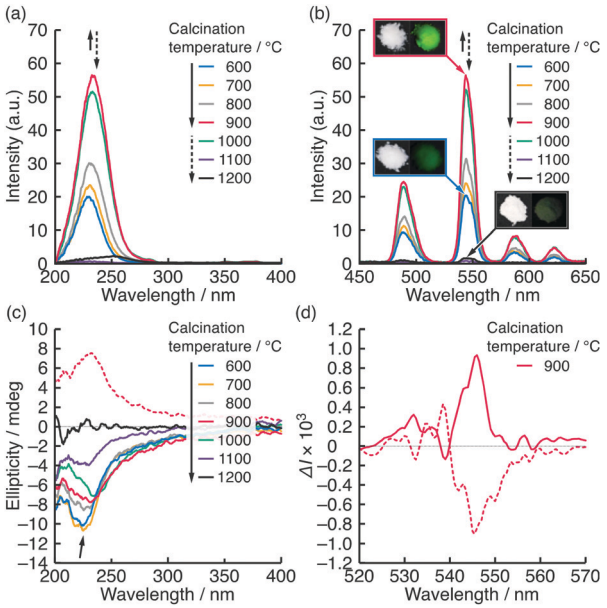

Fig. 3 (a) Excitation, (b) emission, (c) ECD and (d) CPL spectra of SiO_2:Tb^{3+}s calcined at different temperatures (600–1200 °C); measurement temperature: 25 °C, emission wavelength for (a): 544 nm, excitation wavelength for (b) and (d): 230 nm. The spectra of L- and D-SiO_2:Tb^{3+}s are denoted by solid and dashed lines, respectively. Insets in (b) show pictures of L-SiO_2:Tb^{3+}s calcined at 600, 900 and 1200 °C in daylight (left) and under 254 nm UV light in the dark (right). The CPL spectra in (d) were normalized to 1 V of the maximum direct current voltage. The corresponding UV absorption spectra for (c) are shown in Fig. S4 (ESI†). Variations of emission intensity and ellipticity of L-SiO_2:Tb^{3+}s calcined at different temperatures (600–1200 °C) are shown in Fig. S5 (ESI†).

transmission electron microscopy (STEM) observation (Fig. S1a, b, ESI† and Fig. 2a). The obtained silica nanohelices were immersed in terbium(III) acetate aqueous solution (20 mM, 30 mL) for 18 h and thoroughly washed with water until unadsorbed terbium(III) acetate was almost completely removed (typically 6 times washing) as checked by the ultraviolet (UV) absorption spectra (Fig. S2, ESI†). The washed hybrids were freeze dried and then calcined at 600–1200 °C for 4 h in air. When the calcination temperature ranges between 600 and 1000 °C, Tb^{3+}-doped nanosilicas (hereafter, abbreviated as L- and D-SiO_2:Tb^{3+}s prepared from 16-2-16 L- and D-tartrate, respectively) maintained the helical shape (Fig. 2b and Fig. S1c–f, ESI†). When the calcination temperature reached 1100 °C, the helical shape started to melt while keeping the fibrous structure (Fig. 2c). No defined structure was observed anymore when they were calcined at 1200 °C (Fig. 2d). Energy dispersive X-ray (EDX) spectroscopy detected signals ascribed to terbium (Fig. S3, ESI†). The Tb^{3+} concentrations in the nanosilicas calcined at 600–1200 °C were estimated from the EDX results to be around 0.31 at% (2.4 wt%, standard deviation: 0.02 at% and 0.1 wt%, Table S1, ESI†).

Fig. 3a and b show the solid-state excitation and emission spectra, respectively, of L-SiO_2:Tb^{3+}s calcined at different temperatures. SiO_2:Tb^{3+}s showed four sharp emission peaks at 489, 544, 586 and 621 nm (Fig. 3b), which correspond to the transition from the $^5D_4$ state to the ^7F_J (J = 6, 5, 4 and 3) states of Tb^{3+}, respectively.[15–17] In the excitation spectra of L-SiO_2:Tb^{3+}s monitored at 544 nm, excitation bands were observed at around 230 nm (Fig. 3a), which were attributed to the $4f^8 \rightarrow 4f^7 5d$ transition of Tb^{3+}.[16,17] The emission intensity increased with increasing calcination temperature up to 900 °C (Fig. 3b and Fig. S5a, ESI†). This is probably due to the decrease in OH groups of nanosilica with increasing calcination temperature and the resulting reinforced interaction of Tb^{3+} with $(Si–O)_n$.[17] Indeed, the thermal gravimetric analysis (TGA) thermogram showed a gradual weight loss in the temperature range of 600–1100 °C (Fig. S6a, ESI†). Furthermore, the Fourier transform infrared (FTIR) spectra showed a gradual decrease in the peak around 3400 cm^{-1} and a shoulder around 940 cm^{-1} which originates from O–H and Si–OH stretching vibration,[13,17] respectively (Fig. S6b and c, ESI†). Broadening of the excitation bands was simultaneously observed (Fig. 3a) which also confirms the increase of $4f^8 \rightarrow 4f^7 5d$ transition accompanied by the formation of $(Si–O)_n$–Tb^{III} bonds.[17] Over 1000 °C, the emission intensity decreased drastically (Fig. 3b and Fig. S5a, ESI†). The high resolution transmission electron microscopy (HRTEM) observation revealed the presence of crystalline nanoparticles in L-SiO_2:Tb^{3+} when calcined at 1200 °C which showed lattice fringes (Fig. S7b, ESI,† left and middle) and its fast Fourier transform (FFT) pattern exhibited clear diffraction spots (Fig. S7b, ESI,† right). In the same image, the area that did not show lattice fringes also did not show diffraction spots, indicating that silica surrounding the nanoparticles remained amorphous. Meanwhile, for L-SiO_2:Tb^{3+} heated to 900 °C, no lattice fringes and diffraction spots were observed anywhere in the image (Fig. S7a, ESI†). We therefore conclude that the decrease in the emission intensity of SiO_2:Tb^{3+} heated beyond 1000 °C is due to the transformation of individually dispersed Tb^{3+} into nanoparticles, probably as terbium oxide, for which only the Tb atoms in the outer surface can be emissive.

Would such bare Tb^{3+} ions doped in the amorphous helical siloxane network without any organic mediates "feel" the morphological chirality of the surrounding silica helices? We then performed electronic circular dichroism (ECD) spectral measurement using a diffuse reflectance method and circularly polarized luminescence (CPL) spectral measurement of SiO_2:Tb^{3+}s. In the case of silica nanohelices without any doping, a slight monotonous increase with mirror image sign was observed below 250 nm which can be attributed to scattering from chiral silica (Fig. S8d, ESI†). The helical silica immersed in the solution of terbium(III) acetate, SiO_2:Tb^{3+} washed without calcination ([Tb^{3+}] = 0.32–0.33 at%), showed the mirror image ECD signals (Fig. S8d, ESI†) for L- and D-SiO_2:Tb^{3+} which showed a monotonous increase with decreasing wavelength with a slight shoulder at around 225 nm. This increase is likely due to acetate ions entrapped along with Tb^{3+} ions. For the calcined SiO_2:Tb^{3+}s beyond 600 °C the clear ECD signals specific to Tb^{3+} ions were observed centered at around 230 nm (Fig. 3c) close to the absorption and excitation $4f^8 \rightarrow 4f^7 5d$ transition band of Tb^{3+} (Fig. S4, ESI† and Fig. 3a). The ECD signals slightly decreased with increasing calcination temperature (Fig. 3c and Fig. S5b, ESI†). These results suggest that the chiral coordination of Tb^{3+} with Si–O(H) decreased with the increasing calcination temperature, even though their helical shapes were maintained. The linear dichroism (LD) component was negligible for these samples (Fig. S9, ESI†). When the calcination temperature surpassed 1000 °C, the ellipticity decreased strongly and SiO_2:Tb^{3+} calcined at 1200 °C hardly exhibited the ECD signal (Fig. 3c and Fig. S5b, ESI†). As mentioned above, SiO_2:Tb^{3+} calcined at 1100 °C does not maintain a helical shape (Fig. 2c) and SiO_2:Tb^{3+} calcined at 1200 °C no longer has a ribbon-like structure (Fig. 2d). Such a strong correlation between the nanohelical morphology and the ECD signal allows us to conclude that the chiral property of Tb^{3+} comes from the helical silica with a chirally arranged siloxane network surrounding Tb^{3+}, although the ensemble of the silica network is amorphous. We suggest that the 4f orbital of Tb^{3+} is chirally distorted by the effect of the interaction of the chirally arranged Si–O to Tb^{3+}.

The ECD signal was strongly dependent on the Tb^{3+} concentration in the helical silica (Fig. 4). We prepared three different concentrations of the terbium(III) acetate solutions (20, 2 and 0.2 mM) during the immersion process. The Tb^{3+} amounts of SiO_2:Tb^{3+} prepared using 20, 2 and 0.2 mM terbium(III) acetate aqueous solutions were evaluated by inductively coupled plasma (ICP) analysis after hydrofluoric acid treatment and estimated to be 0.2, 0.05 and 0.006 at%, respectively (Table S1, ESI†).

Such inorganic ions entrapped in the silica nanohelices also showed CPL signals as shown in Fig. 3d. SiO_2:Tb^{3+}s calcined at 900 °C which were mounted in a 0.01 cm path length quartz cell showed the mirror image CPL signals at around 545 nm when irradiated at 230 nm. The dissymmetry factor was estimated to be $|1 \times 10^{-3}|$. Different from the ECD measurements, the CPL signals were not detectable for SiO_2:Tb^{3+} calcined at lower temperature such as 600 °C probably due to the low emission intensity.

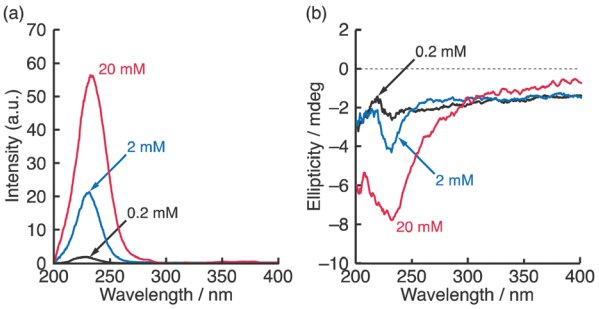

Fig. 4 (a) Excitation and (b) ECD spectra of L-SiO_2:Tb^{3+}s calcined at 900 °C which were prepared using 20, 2 and 0.2 mM terbium(III) acetate aqueous solution in the immersion process; measurement temperature: 25 °C, emission wavelength for (a): 544 nm. The corresponding emission and UV absorption spectra are shown in Fig. S10 (ESI†).

We have previously reported that the chiral morphology of the self-assemblies of 16-2-16 tartrate evolve with time.[18] Indeed, in the early stage of the helical formation, twisted ribbons with Gaussian curvature are observed, which then transform to helical ribbons with a cylindrical curvature within hours to days. In the present study, we compared the effect of the nature of the curvature of chiral nanosilicas, twisted *vs.* helical ones formed from the same molecules, on the chiroptical properties of Tb^{3+} entrapped within. The twisted nanosilica was prepared with 1.5 h aging time of 16-2-16 tartrate aqueous dispersion.[4,6,7,11–13] The twisted SiO_2:Tb^{3+} calcined at 900 °C ([Tb^{3+}] = 0.37–0.40 at%) also showed characteristic emission (Fig. S11a, ESI†) and ECD signal around 230 nm (Fig. 5b) close to the absorption and excitation bands (Fig. S11b, ESI† and Fig. 5a). It is noted that the ECD signal of the twisted SiO_2:Tb^{3+} was weaker than that of the helical one (Fig. 5b), despite the fact that the emission intensity of the twisted SiO_2:Tb^{3+} was a little stronger with slightly higher concentration of Tb^{3+} in the twisted ribbons (Fig. S11a, ESI†). This can be due to the weaker chiral ordering of Si–O(H) on the surface of the twisted nanosilica which is made from the chiral template with a shorter aging time, and/or the intrinsic nature of the twisted ribbons with the given pitch shows lower effect to

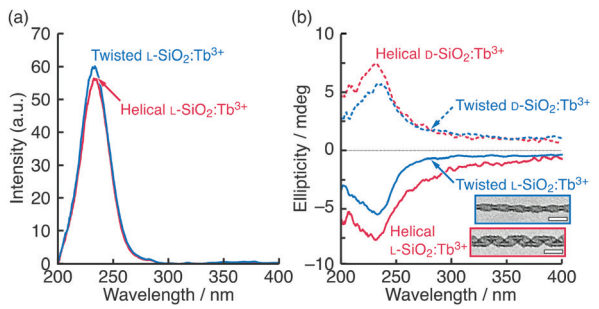

Fig. 5 (a) Excitation and (b) ECD spectra of the twisted and helical SiO_2:Tb^{3+}s calcined at 900 °C; measurement temperature: 25 °C, emission wavelength for (a): 544 nm. Insets in (b) show STEM images of the helical and twisted L-SiO_2:Tb^{3+}. The scale bars indicate 50 nm. The corresponding emission and UV absorption spectra are shown in Fig. S11 (ESI†).

induce the chiral environment to the entrapped ions in the network.

This method to induce chiral signals from lanthanide as described above is surprisingly simple. Just immerse the silica nanohelices in the lanthanide salt solution, wash away the non-adsorbed salt, then calcine them. In order to verify if this observation can be generalized with other lanthanide ions, we prepared Eu^{3+}-doped helical nanosilica (hereafter, abbreviated as SiO_2:Eu^{3+}). The SiO_2:Eu^{3+} ([Eu^{3+}] = 0.32–0.35 at%) also showed characteristic emission with a peak at 616 nm ascribed to the Eu^{3+} $^5D_0 \rightarrow {}^7F_2$ transition[16] and the ECD signal below 250 nm (Fig. S12b and d, ESI†), although CPL signals could not be detected because of the low emission intensity. The ECD band is close to the absorption and excitation bands (Fig. S12a, c and d, ESI†) and therefore can be ascribed to the charge transfer process between Eu^{3+} and chirally coordinated oxygen atoms.[16]

In conclusion, chiroptical properties were successfully induced to lanthanide ions doped in silica nanohelices with a chirally arranged siloxane network in the absence of any organic molecules, demonstrating direct chirality induction to inorganic ions by chiral inorganic solids. This induction was observed at very low atomic concentration such as 0.3 at% and was still clearly observable. We suggest that the inorganic silica acts as a chiral ligand for Tb^{3+}. This in turn shows that the lanthanide ions doped in the silica network can play a role to probe the degree of the chiral order of Si–O(H). Such findings lead to the better understanding of the chirality of inorganic materials and also provide a new strategy for the design of inorganic luminescent optically active materials.

This work was supported by the "Japan Society for the Promotion of Science, Grant-in-Aid for Scientific Research (C), Grant Number 17K05000", the Centre National de la Recherche Scientifique and Université de Bordeaux for the "French-Japanese International Associated Laboratory, Chiral Nanostructures for Photonic Applications (LIA-CNPA)". We are grateful to T. Kiyomura of Institute for Chemical Research, Kyoto University for HRTEM observation, which was supported by Kyoto University Nano Technology Hub in Nanotechnology Platform Project sponsored by the Ministry of Education, Culture, Sports, Science and Technology (MEXT), Japan, Grant Number A-20-KT-0020.

Conflicts of interest

There are no conflicts to declare.

Notes and references

1 (*a*) N. Kameta, M. Masuda and T. Shimizu, *Chem. Commun.*, 2016, **52**, 1346; (*b*) K. Maeda and E. Yashima, *Top. Curr. Chem.*, 2017, **375**, 72; (*c*) N. Ryu, Y. Okazaki, E. Pouget, M. Takafuji, S. Nagaoka, H. Ihara and R. Oda, *Chem. Commun.*, 2017, **53**, 8870; (*d*) Y. Nagata, R. Takeda and M. Suginome, *ACS Cent. Sci.*, 2019, **5**, 1235.

2 (*a*) M. Naito, K. Iwahori, A. Miura, M. Yamane and I. Yamashita, *Angew. Chem., Int. Ed.*, 2010, **49**, 7006; (*b*) Y. Duan, L. Han, J. Zhang, S. Asahina, Z. Huang, L. Shi, B. Wang, Y. Cao, Y. Yao, L. Ma, C. Wang, R. K. Dukor, L. Sun, C. Jiang, Z. Tang, L. A. Nafie and S. Che, *Angew. Chem., Int. Ed.*, 2015, **54**, 15170; (*c*) J. Kumar, T. Kawai and T. Nakashima, *Chem. Commun.*, 2017, **53**, 1269; (*d*) W. Ma, L. Xu, A. F. de Moura, X. Wu, H. Kuang, C. Xu and N. A. Kotov, *Chem. Rev.*, 2017, **117**, 8041; (*e*) X. Jin, Y. Sang, Y. Shi, Y. Li, X. Zhu, P. Duan and M. Liu, *ACS Nano*, 2019, **13**, 2804.

3 (*a*) H. Qiu, Y. Inoue and S. Che, *Angew. Chem., Int. Ed.*, 2009, **48**, 3069; (*b*) J. Jiang, T. Wang and M. Liu, *Chem. Commun.*, 2010, **46**, 7178; (*c*) R.-H. Jin, D.-D. Yao and R. Tamoto Levi, *Chem. – Eur. J.*, 2014, **20**, 7196; (*d*) S. Tsunega, R.-H. Jin, T. Nakashima and T. Kawai, *ChemPlusChem*, 2019, **84**, 1.

4 A. Scalabre, A. M. Gutiérrez-Vílchez, Á. Sastre-Santos, F. Fernández-Lázaro, D. M. Bassani and R. Oda, *J. Phys. Chem. C*, 2020, **124**, 23839.

5 M. Sugimoto, X.-L. Liu, S. Tsunega, E. Nakajima, S. Abe, T. Nakashima, T. Kawai and R.-H. Jin, *Chem. – Eur. J.*, 2018, **24**, 6519.

6 (*a*) J. Cheng, G. Le Saux, J. Gao, T. Buffeteau, Y. Battie, P. Barois, V. Ponsinet, M.-H. Delville, O. Ersen, E. Pouget and R. Oda, *ACS Nano*, 2017, **11**, 3806; (*b*) M. Attoui, E. Pouget, R. Oda, D. Talaga, G. L. Bourdon, T. Buffeteau and S. Nlate, *Chem. – Eur. J.*, 2018, **24**, 11344; (*c*) P. Liu, W. Chen, Y. Okazaki, Y. Battie, L. Brocard, M. Decossas, E. Pouget, P. Müller-Buschbaum, B. Kauffmann, S. Pathan, T. Sagawa and R. Oda, *Nano Lett.*, 2020, **20**, 8453.

7 R. Oda, E. Pouget, T. Buffeteau, S. Nlate, H. Ihara, Y. Okazaki and N. Ryu, in *Molecular Technology, Materials Innovation*, ed. H. Yamamoto and T. Kato, Wiley-VCH, Weinheim, 2019, ch. 6, vol. 3, pp. 107–136.

8 (*a*) C. Baleizão, B. Gigante, D. Das, M. Alvaro, H. Garcia and A. Corma, *Chem. Commun.*, 2003, 1860; (*b*) T. Ooi and K. Maruoka, *Angew. Chem., Int. Ed.*, 2007, **46**, 4222; (*c*) P. Wang, X. Liu, J. Yang, Y. Yang, L. Zhang, Q. Yang and C. Li, *J. Mater. Chem.*, 2009, **19**, 8009.

9 J. J. Bodwin, A. D. Cutland, R. G. Malkani and V. L. Pecoraro, *Coord. Chem. Rev.*, 2001, **216–217**, 489.

10 (*a*) J. Kumar, B. Marydasan, T. Nakashima, T. Kawai and J. Yuasa, *Chem. Commun.*, 2016, **52**, 9885; (*b*) T. Wu and P. Bouř, *Chem. Commun.*, 2018, **54**, 1790; (*c*) Y. Hasegawa, Y. Miura, Y. Kitagawa, S. Wada, T. Nakanishi, K. Fushimi, T. Seki, H. Ito, T. Iwasa, T. Taketsugu, M. Gon, K. Tanaka, Y. Chujo, S. Hattori, M. Karasawa and K. Ishii, *Chem. Commun.*, 2018, **54**, 10695; (*d*) F. Zinna, L. Arrico and L. D. Bari, *Chem. Commun.*, 2019, **55**, 6607; (*e*) L. Arrico, L. D. Bari and F. Zinna, *Chem. – Eur. J.*, 2021, **27**, 2920.

11 (*a*) K. Sugiyasu, S.-i. Tamaru, M. Takeuchi, D. Berthier, I. Huc, R. Oda and S. Shinkai, *Chem. Commun.*, 2002, 1212; (*b*) Y. Okazaki, J. Cheng, D. Dedovets, G. Kemper, M.-H. Delville, M.-C. Durrieu, H. Ihara, M. Takafuji, E. Pouget and R. Oda, *ACS Nano*, 2014, **8**, 6863; (*c*) Y. Okazaki, N. Ryu, T. Buffeteau, S. Pathan, S. Nagaoka, E. Pouget, S. Nlate, H. Ihara and R. Oda, *Chem. Commun.*, 2018, **54**, 10244; (*d*) N. Ryu, T. Kawaguchi, H. Yanagita, Y. Okazaki, T. Buffeteau, K. Yoshida, T. Shirosaki, S. Nagaoka, M. Takafuji, H. Ihara and R. Oda, *Chem. Commun.*, 2020, **56**, 7241; (*e*) W. Yospanya, M. Nishijima, Y. Araki, T. Buffeteau, E. Pouget, T. Wada and R. Oda, *Chem. Commun.*, 2020, **56**, 10058.

12 N. Ryu, Y. Okazaki, K. Hirai, M. Takafuji, S. Nagaoka, E. Pouget, H. Ihara and R. Oda, *Chem. Commun.*, 2016, **52**, 5800.

13 Y. Okazaki, T. Buffeteau, E. Siurdyban, D. Talaga, N. Ryu, R. Yagi, E. Pouget, M. Takafuji, H. Ihara and R. Oda, *Nano Lett.*, 2016, **16**, 6411.

14 (*a*) D. Chen, H. Miyoshi, T. Akai and T. Yazawa, *Appl. Phys. Lett.*, 2005, **86**, 231908; (*b*) Y. Qiao, H. Chen, Y. Lin, Z. Yang, X. Cheng and J. Huang, *J. Phys. Chem. C*, 2011, **115**, 7323.

15 (*a*) H. Lin, E. Y.-B. Pun, X. Wang and X. Liu, *J. Alloys Compd.*, 2005, **390**, 197; (*b*) M. Yang, Y. Liang, Q. Gui, B. Zhao, D. Jin, M. Lin, L. Yan, H. You, L. Dai and Y. Liu, *Sci. Rep.*, 2015, **5**, 11844; (*c*) Z. Jia and M. Xia, *Sci. Rep.*, 2016, **6**, 33283; (*d*) T. Kataoka, K. Shiba, L. Y. Wang, S. Yamada and M. Tagaya, *RSC Adv.*, 2017, **7**, 19479.

16 (*a*) R. Reisfeld, *J. Res. Natl. Bur. Stand., Sect. A*, 1972, **76**, 613; (*b*) X. Kang, S. Huang, P. Yang, P. Ma, D. Yang and J. Lin, *Dalton Trans.*, 2011, **40**, 1873.

17 Q. Guodong, W. Minquan, W. Mang, F. Xianping and H. Zhanglian, *J. Lumin.*, 1997, **75**, 63.

18 (*a*) R. Oda, F. Artzner, M. Laguerre and I. Huc, *J. Am. Chem. Soc.*, 2008, **130**, 14705; (*b*) J. Gao, Y. Okazaki, E. Pouget, S. Nlate, B. Kauffmann, F. Artzner, T. Buffeteau and R. Oda, *Mater. Chem. Front.*, 2021, DOI: 10.1039/d0qm00989j.